Dynamics of Tryptophan in the Histidine-Containing Phosphocarrier Protein of *Streptomyces coelicolor*: Evidence of Multistate Equilibrium Unfolding†

José A. Poveda,*,‡ Gregorio Fernández-Ballester,‡ Manuel Prieto,§ and José L. Neira*,‡,||

Instituto de Biología Molecular y Celular, Universidad Miguel Hernández, 03202 Elche (Alicante), Spain, Centro de Química-Física Molecular, Instituto Superior Técnico, P-1049-001 Lisbon, Portugal, and Instituto de Biocomputación y Física de los Sistemas complejos, 50009 Zaragoza, Spain

Received February 10, 2007; Revised Manuscript Received April 10, 2007

ABSTRACT: The nanosecond dynamics of the single tryptophan, Trp10, of HPr from *Streptomyces coelicolor*, HPr^{sc}, has been monitored at different pHs. Time-resolved fluorescence methods and DOSY measurements have been used to map the compactness of the protein. At low pHs, where a molten globule-like species has been described, the correlation times from fluorescence showed an abrupt change as the pH was increased. When the protein was folded (above pH 4), two correlation times were observed, which remained practically constant up to pH 9.5. The long correlation time, around 7.5 ns, corresponds to the global rotational motion of the protein, since this value is in agreement with that determined theoretically from hydrodynamic measurements. The short correlation time, around 1.4 ns, must report on fast movements of the protein segment containing the tryptophan residue. On the other hand, fluorescence lifetimes showed the same abrupt change as the correlation times at low pH, but, in addition, a sigmoidal change with a p$K_a \sim 4.3$ was also observed. On the basis of the modeled structure of HPr^{sc}, this last transition could be due to the proximity of Glu12 to Trp10. The changes monitored by the fluorescence lifetimes agree with those observed previously by steady-state fluorescence, CD, and ANS binding experiments. Taken together, these data suggest a multistate equilibrium during folding of HPr^{sc} starting from low pHs.

Protein aggregation is a side reaction that accompanies the folding reactions of many proteins and whose mechanism is poorly understood. Formation of aggregated proteins may be the result of competition between intra- and intermolecular interactions during protein folding (*1*, *2*). This competition can be the consequence of the accumulation of partially folded intermediates that populate protein folding pathways, containing exposed hydrophobic patches (*3*). Aggregation-prone intermediates can occur transiently during folding at any stage (*4*, *5*), and they can transform to native protein without first undergoing unfolding. Many proteins unfold to partially unfolded forms, with exposed hydrophobic patches at low pH (*6*), and then show a strong tendency to aggregate. For instance, a partially folded form, in dynamic equilibrium with the native state of the protein, self-associates and initiates fibril formation in human lysozyme at high pH values (*7*), and amyloid fibril formation in vitro of transthyretin results from the self-assembly of an intermediate formed during partial acid denaturation of the protein (*8*). Indeed, aggregation leading to amyloid fibril deposition in neurodegenerative diseases involves, in most cases, unfolding of a normally folded protein under low pH conditions (*3*).

The histidine-containing phosphocarrier protein of *Streptomyces coelicolor*, HPr^{sc},[1] unfolds reversibly at low pH. This protein plays a key role in the transport of carbohydrates across cell membranes of bacteria via the phosphoenolpyruvate-dependent sugar phosphotransferase system (PTS) (*9*, *10*). HPr^{sc} catalyzes the transfer of a phosphoryl group from enzyme I to enzyme II, the membrane-bound transporter. The presence of PTS in *S. coelicolor* has been reported, and the corresponding proteins have been cloned and expressed (*11*−*13*). HPr^{sc} contains 93 amino acid residues; it lacks cysteine and tyrosine residues, and it only contains one tryptophan and one phenylalanine residue. The structures of HPr proteins from several species have been described by NMR spectroscopy (refs *14*−*16* and references cited therein) and X-ray diffraction (*17*, *18*). Those structures show a classical open-face β-sandwich fold consisting of three α-helices packed against a four-stranded antiparallel β-sheet. The NMR assignments of HPr^{sc} indicate that its structure is similar to that observed in other members of the HPr family (unpublished results). We have shown that HPr^{sc} forms a partially unfolded form at pH 3, which is devoid of defined tertiary interactions, as shown by fluorescence and ANS binding experiments; furthermore, some of its secondary structure is lost, as shown by CD and FTIR (*19*). Thus, the

† This work was supported by Projects CTQ2005-00360/BQU from the Spanish Ministerio de Educación y Ciencia (to J.L.N.) and POCI/SAL-FCT/5714/2004 from the Portuguese Ministry of Science (to M.P.). J.A.P. was the recipient of a short-term EMBO fellowship.

* Corresponding authors. J.A.P.: tel, +34 966658466; fax, +34 966658758; e-mail, ja.poveda@umh.es. J.L.N.: tel, +34 966658459; fax, +34 966658758; e-mail, jlneira@umh.es.

‡ Universidad Miguel Hernández.

§ Instituto Superior Técnico.

|| Instituto de Biocomputación y Física de los Sistemas complejos.

[1] Abbreviations: ANS, 8-anilino-1-naphthalenesulfonate; CD, circular dichroism; DOSY, diffusion ordered spectroscopy; FTIR, Fourier transform infrared spectroscopy; HPr, histidine-containing phosphocarrier protein; HPr^{sc}, histidine-containing phosphocarrier protein from *Streptomyces coelicolor*; NATA, *N*-acetyl-L-tryptophanamide; NMR, nuclear magnetic resonance spectroscopy; PTS, the phosphoenolpyruvate-dependent sugar phosphotransferase system.

10.1021/bi7002923 CCC: $37.00
Published on Web 05/22/2007

partially unfolded form at low pH has the features of the so-called molten globule species. However, we did not know whether this molten globule-like species does aggregate or has an extended shape, since it eluted at the void volume of the column during the gel filtration experiments (*19*). If the molten globule-like species was a soluble aggregate, its presence must precede the final formation of a putative insoluble aggregate, and then, the structural characterization of a soluble protein aggregate should be useful in the study of the early structural changes that eventually lead to irreversible protein aggregation. Furthermore, the mechanism of formation of molten globule species, either from soluble aggregated forms or from one single molecule species, is also poorly understood. An understanding of the forces leading to the formation of the molten globule state will help to a better description of the folding process.

To address some of these questions, we have carried out a study of the low-pH denatured species of HPr^{sc} by using time-resolved fluorescence lifetime and anisotropy measurements and DOSY-NMR experiments. Further, we have modeled the structure of the protein to provide clues about which residues are involved during the folding reaction starting from low pH. The highly sensitive fluorescence properties of Trp10 have been exploited to provide information about protein structural and dynamic changes during the folding reaction, while NMR self-diffusion measurements provide information on the compactness of these species. The results from both techniques indicate that the protein at low pH is an oligomer and that the folding of HPr^{sc}, as monitored by time-resolved fluorescence, occurs through a multistate equilibrium.

EXPERIMENTAL PROCEDURES

Materials. Deuterium oxide was obtained from Apollo Scientific, and sodium trimethylsilyl[2,2,3,3-$^2H_4$]propionate (TSP) was from Sigma. Imidazole, Trizma acid, its base, and NaCl were from Sigma. β-Mercaptoethanol was from Bio-Rad, and the Ni^{2+} resin was from Invitrogen. Dialysis tubing was from Spectrapore with a molecular mass cutoff of 3500 Da. Standard suppliers were used for all other chemicals. Water was deionized and purified on a Millipore system.

Protein Expression and Purification. The HPr clone comprises residues 1−93, with the extra methionine and the His_6 tag at the N terminus. We have carried out all of the studies with this construction since its structure, as observed by NMR (unpublished results), is similar to that found in other members of the HPr family and the His_6 tag is disordered in solution, making no contacts with the rest of the protein. Furthermore, stability measurements and biophysical characterization have shown no differences between the His-tagged protein and that where the His tag had been removed (*19*). Recombinant protein was expressed and purified as described (*19*). Protein was more than 99% pure as judged by SDS protein-denaturing gels. The samples were dialyzed extensively against water and stored at −80 °C. Protein concentration was calculated from the absorbance of stock solutions measured at 280 nm, using the extinction coefficients of model compounds (*20*).

Translational Diffusion Measurements (DOSY Experiments). Translational self-diffusion measurements were performed by using the pulsed-gradient spin−echo NMR method (*21*, *22*). The following relationship exists between the translational self-diffusion parameter, *D*, and the NMR parameters (*21*, *22*):

$$\frac{I}{I_0} = -\exp\left[D\gamma_H{}^2\delta^2G^2\left(\Delta - \frac{\delta}{3} - \frac{\tau}{2}\right)\right] \quad (1)$$

where I is the measured peak intensity of a particular (or a group of) resonance(s), I_0 is the maximum peak intensity of the same resonance(s) at the smaller gradient strength, D is the translational self-diffusion constant (in $cm^2\ s^{-1}$), γ_H is the magnetogyric constant of the proton, δ is the duration (in s) of the gradient, G is the strength of the gradient (in T cm^{-1}), Δ is the time (in s) between the gradients, and τ is the recovery delay between the bipolar gradients (100 μs). Data are plotted as the $-\ln(I/I_0)$ versus G^2, and the slope of the line is $D\gamma_H{}^2\delta^2[\Delta - (\delta/3) - (\tau/2)]$, from where D can be easily obtained.

The Stokes−Einstein equation relates D to R, the hydrodynamic radius of a sphere, and the viscosity of the solvent, η, according to

$$R = kT/(6\pi\eta D) \quad (2)$$

where T is the temperature and k the Boltzmann constant.

The viscosity of a solution is very weakly influenced by the macromolecule component at the concentrations used, and therefore, the viscosity of the solution is that of the solvent. Solvent viscosity is temperature-dependent according to the equation (*23*) $\log \eta = a + [b/c - T]$. The terms a, b, and c are given for a particular D_2O:H_2O ratio. In our conditions, a 100% D_2O solution, the values were $a = -4.2911$, $b = -164.97$, and $c = 174.24$. This yields a value of $\eta = 1.253$ kg/(cm s) at 293 K, used in our calculations.

The gradient strength was calibrated by using the diffusion rate for the residual proton water line in a sample containing 100% D_2O in a 5 mm tube and back-calculating G. This procedure assumes that the diffusion rate for HDO in a 100% D_2O sample is 1.94×10^{-5} $cm^2\ s^{-1}$ at 298 K (*23*). Experiments were acquired by using the longitudinal eddy current delay pulse sequence, with a postgradient eddy current relaxation delay of 5 ms. Each experiment was averaged over 128 scans, and the number of points was 16 K. The strength of the gradients was varied from 2% of the total power of the gradient coil to 95%, and their shape was a sine function. The largest protein concentration used was 1 mM. The other concentrations were obtained by stock dilution; usually, four different concentrations were used for each pH. For the experiments at the low pHs (2.5 and 3.2), the duration of the gradient was varied between 4.0 and 3.5 ms, and the time between both gradients was changed between 250 and 200 ms; for the experiments at the rest of the pHs, the duration of the gradient was varied between 2.7 and 2.0 ms, and the time between both gradients was modified between 150 and 100 ms. The most upfield shifted methyl groups (between 0.5 and −0.1 ppm for the folded protein and between 1.0 and 0.7 ppm for the unfolded protein) were used to measure the changes in intensity.

Absorption and Fluorescence Spectroscopy. Absorption spectra were acquired in a CAMSPEC M350 spectrophotometer. Steady-state fluorescence measurements were recorded with a SLM-8000C spectrofluorometer.

The decay of the total fluorescence intensity and those of the parallel and perpendicular components were recorded either in a stroboscopic-based (*24*, *25*) fluorescence lifetime instrument (Photon Technology International Inc.) or in a single-photon timing system as previously described (*26*). In the former the light source was a GL-330 pulsed nitrogen laser pumping a GL-302 high-resolution dye laser. The dye laser output at 590 nm was tuned to 295 nm through a frequency doubler (GL-303) and coupled to the sample compartment via fiber optics. The emission at 345 nm was detected through a stroboscopic detector equipped with a photomultiplier, using 1000 channels with a time scaling of 14.5 ps. In the second system, the sample was excited at 295 nm through a frequency-doubled, cavity dumped (3.7 MHz repetition rate), dye laser of Rhodamine 6G (Coherent 701-2), synchronously pumped by a mode-locked Ar^+ laser (514.5 nm; Coherent Innova 400-10). The emission was detected by a Hamamatsu R-2809 MCP photomultiplier at 345 nm (Jobin-Yvon HR320 monochromator). The time scaling was 10−12 ps per channel depending on the pH, and 1024 channels were in use. In either case, the instrumental response function was generated from a scatter dispersion (silica, colloidal water solution). In fluorescence lifetime measurements, the emission was monitored at the magic angle (54.7°) to eliminate the contribution from the decay in anisotropy. Experiments were carried out at 293 K.

The kinetic parameters of the decay of the fluorescence intensity (lifetimes, τ_i, and normalized amplitudes, α_i) were determined by using nonlinear least-squares regression methods to

$$I(t) = \sum_i \alpha_i \exp(-t/\tau_i) \tag{3}$$

where $I(t)$ is the fluorescence intensity at time t. The average fluorescence lifetime, $\langle\tau\rangle$, was calculated as (*27*)

$$\langle\tau\rangle = \sum_i \alpha_i \tau_i^2 / \sum_i \alpha_i \tau_i \tag{4}$$

The anisotropy decay parameters (rotational correlation times, φ_i, amplitudes, β_i, initial anisotropy, r_0, and residual anisotropy, r_∞) were determined using a nonlinear least-squares global analysis method by simultaneously fitting the vertically and horizontally polarized emission components to a sum of exponentials and a constant term (*28*, *29*):

$$r(t) = (r_0 - r_\infty)[\sum_i \beta_i \exp(-t/\varphi_i)] + r_\infty \tag{5}$$

where $\sum_i \beta_i = 1$.

For the fluorescence lifetime and the anisotropy parameters, the best fit of the theoretical curve to the data was evaluated from the usual statistical criteria, namely, a reduced χ^2 value lower than 1.3 and a random distribution of weighted residuals.

At pHs where two different correlation times were observed, the total anisotropy can be interpreted as the product of two independent depolarizing processes: a first one due to fast movements of a protein segment containing the tryptophan residue, $r'(t)$, and a second one related to the global rotational motion of the whole peptide (*30*), $r(t)$:

$$r(t) = r'(t) \exp(-t/\varphi_{\text{global}})$$

$$r'(t) = r_0[(1 - S^2) \exp(-t/\varphi_{\text{segmental}}) + S^2] \tag{6}$$

The short and long rotational correlation times obtained from the fit of eq 5 to the experimental data are related to φ_{global} and $\varphi_{\text{segmental}}$ by $\varphi_{\text{long}} = \varphi_{\text{global}}$ and $\varphi_{\text{short}} = \varphi_{\text{segmental}}\varphi_{\text{global}}/(\varphi_{\text{segmental}} + \varphi_{\text{global}})$. S is the order parameter characterizing the fluctuation of the protein monitored by the tryptophan; a value close to 1 indicates that the particular region of the macromolecule is very rigid, and a value close to zero indicates a high mobility.

If three correlation times were needed, a similar data analysis was carried out. We considered three independent depolarizing processes; two of them were due to fast movements of protein segments containing the tryptophan residue, and the third one was related to the global rotational motion of the peptide.

For segmental motions, the average angular displacement of these motions was calculated by the model of isotropic diffusion inside a cone (*31*). The cone angle, Θ, was calculated as

$$\cos \Theta_0 = {}^1/_2[(8S + 1)^{1/2} - 1] \tag{7}$$

Modeled Structure. The HPr^{sc} was modeled by homology modeling using the templates available in the Protein Data Bank (http://www.rcsb.org/pdb). The models were constructed with the SWISS MODEL Server (*32*) using the high-resolution HPr protein from *Mycoplasma capricolum* (PDB accession code 1PCH). Sequence alignment was made with CLUSTALW at the EBI site (http://www.ebi.ac.uk) by using the Needleman−Wunsch global alignment algorithm. The HPr proteins from *S. coelicolor* and *M. capricolum* share 23.5% identity and 44.9% similarity, with the positions at the active site fully conserved. This is not surprising since the HPr from *Mycoplasma* resembles HPrs from Gram-positive bacteria more closely than those from Gram-negative bacteria (*33*). The orientation and optimization of the side chains were carried out in two steps: first, those residues making van der Waals clashes were selected and fitted with "Quick and Dirty" algorithms; second, models were energy minimized (100 steps of steepest descent and 100 conjugate gradient, cutoff of 10 Å for nonbonded interactions) with Insight II (Biosym/MSI). Structure edition was made with Swiss PDB viewer v3.7 (*34*) and Insight II (Accelrys Software Inc., http://www.accelrys.com/). The model was tested in terms of energy with Fold-X (*35*, *36*) (at the EMBL site: http://foldx.embl.de); this program evaluates the properties of the structure, such as its atomic contact map, the accessibility of the atoms and residues, the backbone dihedral angles, and the hydrogen bond and electrostatic networks of the protein. In addition, the model was evaluated with PROCHECK (*37*) showing a Ramachandran plot with 88.0% of the residues in the most favorable regions and 10.6% in the additionally allowed regions. Molecular graphics were created with PyMOL (http://www.pymol.org).

RESULTS

Diffusion Measurements. The 1D-NMR experiments at low pHs (pH 2.5 and 3.2) showed that, at any concentration, the

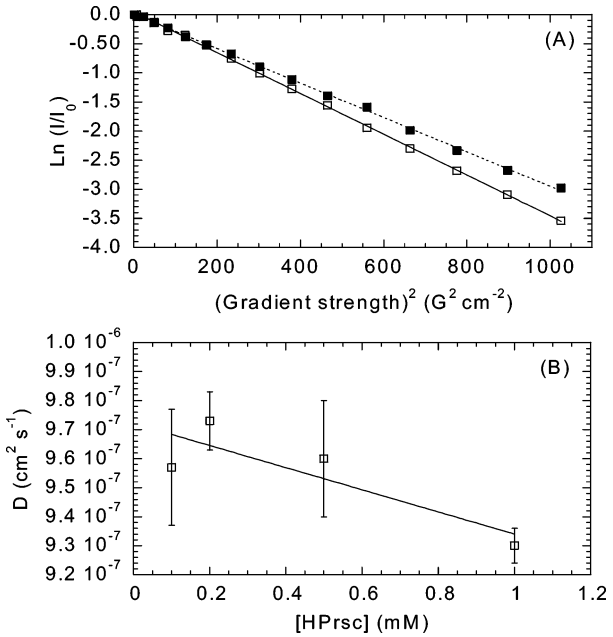

FIGURE 1: DOSY-NMR experiments of HPr^{sc}. (A) The logarithm of the normalized intensity of the most upfield shifted peaks is shown as a function of the square of the gradient strength at two concentrations: 1 mM (continuous line and open squares) and 500 μM (dotted line and filled squares) at pH 4.5. The slopes of the plots give the apparent diffusion constant of the molecule, *D*, in solution at the particular concentration used. (B) NMR diffusion coefficients of the protein as a function of protein concentration at pH 4.5. The bars are fitting errors to eq 1. The solid line is the fitting to a linear equation whose *y*-axis intersection yields the diffusion coefficient at 0 M protein concentration.

Table 1: Diffusion Coefficients (*D*) and Hydrodynamic Radii (*R*) of HPr^{sc} at Different pHs[a]

pH	$D \times 10^7$ (cm^2/s)	*R* (Å)
2.5	3.3 (±0.2)	52.0 (±0.5)
3.2	3.4 (±0.5)	51.8 (±0.5)
3.9	9.8 (±0.5)	17.5 (±0.5)
4.5	9.7 (±0.2)	17.4 (±0.2)
5.6	9.5 (±0.5)	18.0 (±0.5)
6.8	9.8 (±0.1)	17.5 (±0.1)
7.5	9.7 (±0.2)	17.6 (±0.2)

[a] The errors of the *D* measurements come from the fit to a straight line of the experimentally obtained *D* at different concentrations. Errors for the value of *R* come from the propagation errors in eq 2. Measurements were carried out at 293 K.

tertiary structure had been disrupted as judged by the absence of upfield-shifted methyl protons. The signals of the unfolded protein could be clearly observed, although they were broader than those of the folded protein (data not shown).

The translational diffusion coefficient of HPr^{sc} at any of the explored pHs increased linearly as the protein concentration decreased (Figure 1B), since at lower protein concentrations, the molecular impairment of the translational diffusion was smaller. The extrapolated diffusion coefficients at infinite dilution of the protein (i.e., the *y*-axis intersection) are shown in Table 1. The hydrodynamic radii for a spherical HPr^{sc} under any of the explored pHs, *R*, are also shown in Table 1 (obtained from eq 2). Under native conditions (pH 7), the *R* value agrees very well with those determined from gel filtration experiments (16.4 Å) (*19*) and from the modeled structure, 19.1 Å (see below).

Table 2: Fluorescence Lifetime Measurements of HPr^{sc} at Different pHs[a]

pH	α_1	τ_1	α_2	τ_2	α_3	τ_3	χ^2	$\langle t \rangle$
2.38	0.17	0.5	0.54	1.3	0.29	2.8	1.0	2.0
2.58	0.41	0.3	0.44	1.5	0.16	3.1	1.1	2.0
3	0.47	1.0	0.32	2.1	0.22	3.9	1.0	2.6
3.11	0.34	0.9	0.3	1.7	0.36	3.8	1.1	2.9
3.58	0.4	0.3	0.31	1.5	0.28	3.8	1.1	2.8
3.64	0.51	0.9	0.27	2.4	0.22	4.1	1.0	2.8
4.09	0.43	0.6	0.32	1.5	0.25	3.7	1.1	2.6
4.54	0.55	0.3	0.3	1.5	0.15	3.8	1.1	2.5
4.85	0.46	0.9	0.26	1.5	0.28	3.5	1.1	2.5
6.4	0.45	0.4	0.36	1.3	0.19	3.3	1.0	2.2
6.88	0.54	0.3	0.3	1.3	0.16	3.4	1.0	2.2
8.76	0.52	0.4	0.29	1.5	0.19	3.4	1.1	2.3

[a] α_i, normalized amplitudes; τ_i, fluorescence lifetimes; $\langle \tau \rangle$, average fluorescence lifetime. Measurements were carried out at 293 K.

We can compare the estimated *R* from the above experimental measurements with that obtained theoretically. The theoretical hydrodynamic radius for an ideal unsolvated spherical molecule can be calculated considering that the anhydrous molecular volume, ($M\bar{V}/N$), equals the volume of a sphere (*38*, *39*), yielding $R = (3M\bar{V}/4N\pi)^{1/3}$, where *M* is the molecular weight of the protein, $\bar{V}$ is the partial specific volume of the protein, and *N* is Avogadro's number. The molecular mass of monomeric HPr^{sc} is 11554.0 Da, and $\bar{V} = 0.7509$ cm^3/g, as calculated from amino acid composition (*39*); the equation led to a hydrodynamic radius of 15.1 Å. If we consider a hydration shell water of 2.8 Å (*40*), then the *R* is 17.9 Å, which agrees well with those obtained from diffusion measurements (Table 1) and gel filtration experiments (16.4 Å) (*19*). To explain the larger hydrodynamic radius obtained at low pHs (Table 1), it should be assumed that the molecular mass of a *spherical* protein species under those conditions is 40 times that of a single monomer. However, the presence of such large molecular mass aggregated species would have hampered measurements of the intensity signals in the DOSY-NMR experiments due to signal broadness. Alternatively, the large *R* at those pHs could be due to the random coil-like features of the protein, since, as it has been shown, the protein has lost most of its native tertiary and secondary structure under those conditions (*19*) (see Discussion).

Time-Resolved Fluorescence Spectroscopy. Time-resolved fluorescence spectroscopy reflects the structural complexity of proteins. A tryptophan residue can have several fluorescence lifetimes, among other reasons, due to the existence of different rotameric states of the indole moiety. Every state is represented by a discrete excited-state lifetime (*41*) (and then, by an exponential decay function); the distribution of these states and the value of their lifetimes depend on the protein structure and the environment around the tryptophan. Fluorescence intensity kinetics of the single tryptophan of HPr^{sc} were adequately described by a triexponential in the entire range of pH (eq 3). The reduced χ^2 value, characterizing the goodness of the fit, was always less than 1.1, and the residuals were randomly distributed around zero (Table 2). Attempted fits of one- or two-exponential models to the experimental data resulted in an increase of the χ^2 value (larger than 25%), while four-exponential models led to no significant decrease of χ^2. Then, the simpler triexponential

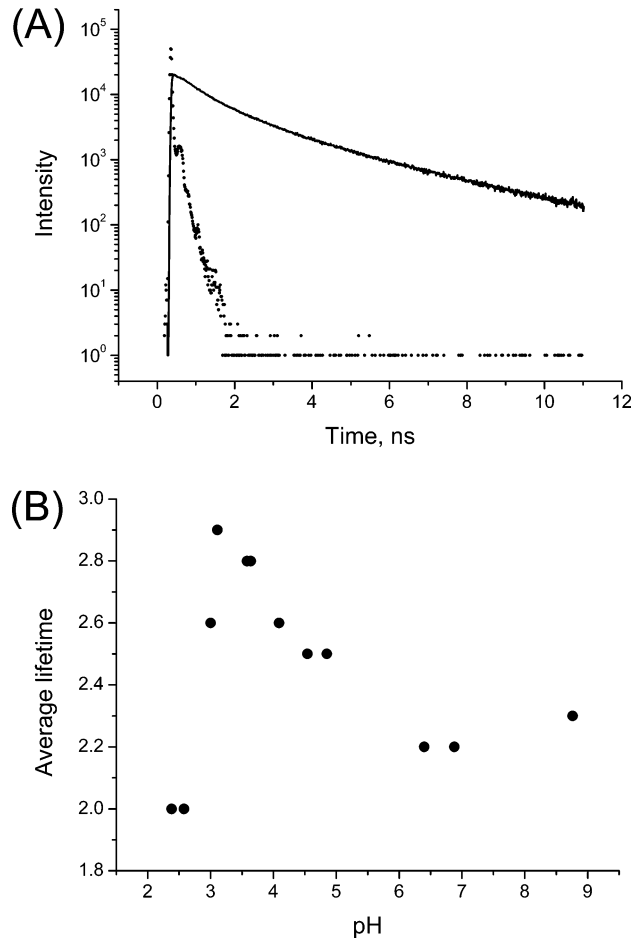

FIGURE 2: Time-resolved fluorescence. (A) Fluorescence intensity decay of HPr^{sc} at pH 6.88. Excitation and emission wavelengths were 295 and 345 nm, respectively. The instrument response function is represented as scattered points. (B) Variation of the HPr^{sc} average lifetime, $\langle\tau\rangle$, with pH.

model was chosen for further consideration. An example of the fit is shown in Figure 2A.

Fluorescence decay of Trp10 was measured at several pHs ranging from 2.38 to 8.76. The fact that there were three exponential functions suggests, even when HPr^{sc} is in a well-folded conformation (at pH 6.88), the existence of ground-state rotamers sensing different chemical environments, which interconvert slowly on the nanosecond time scale (*42*, *43*) (Table 2).

Due to the complexity of the tryptophan fluorescence decay, we decided to use the average lifetime $\langle\tau\rangle$ as the observable parameter at the different pHs (Figure 2B). Two events were, then, observed. The first one had an approximate titration midpoint of p$K_a \sim 3$, and it happened in a very narrow pH range (from 2.4 to 3.5), with a change in $\langle\tau\rangle$ from 2.0 to 2.9 ns. The pK_a of this transition coincides with (i) a large change in the measurements of *D* (see Table 1), (ii) the acquisition of the secondary structure detected from CD (*19*), (iii) a notable blue shift in the fluorescence emission spectra (*19*), and (iv) a strong increase in the average energy of the emission spectra (*19*); the average energy of the emission spectra is defined as $\langle\lambda\rangle = [\sum_1^n(1/\lambda_i)I_i]/\sum_1^n I_i$, where I_i is the fluorescence intensity measured at a wavelength λ_i. On the other hand, the second event had a p$K_a \sim 4.5$, and $\langle\tau\rangle$ decreased smoothly from 2.9 to 2.2 ns in a wide pH range (from 3.5 to 6.0). This event was not accompanied by a

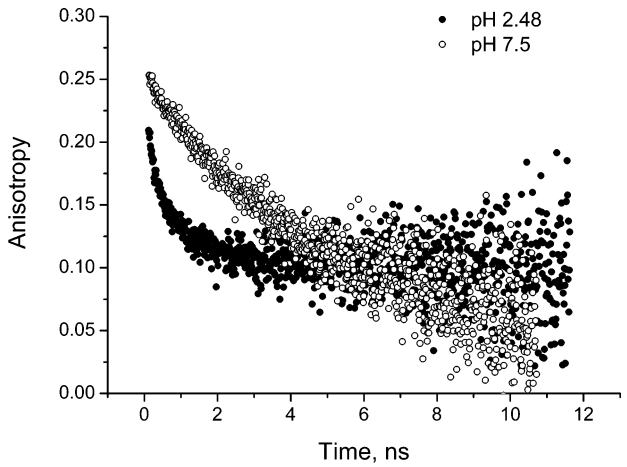

FIGURE 3: Time-resolved fluorescence anisotropy. Time-resolved anisotropy of HPr^{sc} at pH 7.5 and 2.48. Excitation and emission wavelengths were 295 and 345 nm, respectively.

variation in the protein secondary or tertiary structure, although there was a faint drop in the average energy of the emission spectra (*19*).

Finally, a close inspection of the lifetime amplitudes at different pHs (Table 2) let us appreciate that, despite data scattering, α_1 and α_2 crossed over between pH 2 and pH 3.5, while τ_1 and τ_2 remained practically constant. This suggests the interconversion of two species in this pH range, that is, at the same pH range where the first event described above takes place.

Time-Resolved Fluorescence Anisotropy. Time-resolved fluorescence anisotropy monitors the mobility and structural flexibility of proteins. Two correlation times were needed to account for the fluorescence anisotropy decay data at all pHs, except at pH 2.48. In all cases the reduced value of the χ^2 was lower than or equal to 1.1. The attempted fits of the one-exponential model showed a 2-fold increase in the χ^2; on the other hand, addition of another exponential led to no improvement of the χ^2. An example of the decay of fluorescence anisotropy is shown in Figure 3. The parameters associated to the anisotropy decay of Trp10 are summarized in Table 3.

The apparent initial anisotropy, r_0, was around 0.25 at any pH, a value observed in a wide range of peptides and proteins under different solution conditions (*44*, *45*).

At physiological and neutral pHs, where the protein is well folded, two different correlation times were observed. Both values at any pH were larger than 1 ns, and the fast one accounted for 15%, in average, of the whole amplitude. The longer correlation time corresponds to the overall rotational motion of the molecule, whereas the shorter one must correspond to a local independent movement of the polypeptide chain; the *S* order parameter for this local movement is relatively large, yielding small cone angles (Table 3).

Three correlation times (two very short and a very long one) were detected at pH 2.48 (Table 3). The two short correlation times should correspond to fast local movements of the polypeptide chain (see Discussion); the corresponding *S* order parameters for both φ_i were smaller than those calculated at high pH, and then larger cone angles were obtained (Table 3), reflecting less restricted local movements for the tryptophan (eq 7). The long correlation time must correspond to the overall motion of the polypeptide. How-

Table 3: Time-Resolved Fluorescence Anisotropy Parameters of HPr^{sc} at Different pHs[a]

pH	r_0	β_1	φ_1 (ns)	β_2	φ_2 (ns)	β_3	φ_3 (ns)	χ^2	S_1	S_2	Θ_{01}	Θ_{02}	R (Å)
2.48	0.27	0.33	0.08	0.28	0.8	0.40	110	1.1	0.82	0.77	29	33	47.6
3.58	0.26	0.15	1.4	0.85	7.4	0	0	1.1	0.92		19		19.4
4.9	0.24	0.16	1.4	0.84	7.5	0	0	1.0	0.92		19		19.4
6.3	0.26	0.13	1.5	0.87	7.6	0	0	1.1	0.93		17		19.3
7.5	0.25	0.18	1.7	0.82	7.9	0	0	1.1	0.9		21		19.8
9.5	0.25	0.18	1.4	0.82	7.9	0	0	1.1	0.91		21		19.8

[a] r_0, initial anisotropy; β_i, amplitudes; φ_i, rotational correlation times; S_i, order parameter; Θ_{0i}, cone angles; R, hydrodynamic radius obtained from φ_{global}. Measurements were carried out at 293 K.

ever, the calculation of this parameter has a large uncertainty since the tryptophan lifetime is quite short (around 2 ns in average) and then fluorescence intensity is very low at such long times. However, keeping in mind these caveats, and assuming that HPr^{sc} maintains a spherical shape, the calculated R for that correlation time would be 47.6 Å, similar to that derived from the NMR data (Table 1).

Modeled Structure. There are more than 50 HPr molecules and HPr-like templates deposited in the PDB; however, the selection of the template for modeling of HPr^{sc} was restricted due to the presence of Trp10, a position placed in a loop connecting the first β-strand and the first α-helix close to the active site. The loop packs tightly against the C-terminal helix, where position 10 is usually occupied by small amino acids such as Ala, Leu, or Ser (i.e., templates from *Escherichia coli*, *Bacillus subtilis*, *Streptococcus faecalis*, and *Bacillus stearothermophilus*). These templates are incompatible with the presence of bulky amino acids as a tryptophan at position 10, and then, they were not used. In the end, templates having Asp at position 10 (as the HPr from *M. capricolum*), with a more relaxed loop, were able to accommodate the Trp, and they were used to build reliable homology models. The model showed the typical characteristics of HPr structures: (i) the active site His15 end-caps the first α-helix and packs perpendicular to Pro18 (*17*), (ii) Arg17 in the active site is solvent exposed in an typical "open conformation" (*46*), and (iii) Ser47 that end-caps the second α-helix is solvent exposed and susceptible of phosphorylation in Gram-positive bacteria.

Modeling also showed that there were two alternative conformations of the side chain of Trp10. These two conformations also showed two different positions of the His15 side chain, but in both conformers the position of the backbone was not altered. The small hydrophobic pocket close to the C-terminal helix and the active center could be partially solvent-exposed or, alternatively, partially occupied by the Trp10 side chain, thus allowing His15 either to cap the first α-helix (Figure 4A) or to point away to a more solvent-exposed conformation (Figure 4B). The FoldX theoretical energy analysis of both models showed minor differences in stability ($\Delta\Delta G < 2$ kcal/mol), where the salt bridges, as well as the van der Waals interactions, were maintained, and solvation and hydrogen bonds accounted for the very small energy differences. These theoretical findings open the possibility of the coexistence of two alternative conformations of Trp10 that could account for the multiexponential behavior of fluorescence intensity kinetics, although, as indicated above, the existence of ground-state rotamers for one species could also explain it. The presence of these two conformations should also lead to the detection of two different local rotational motions in the native state,

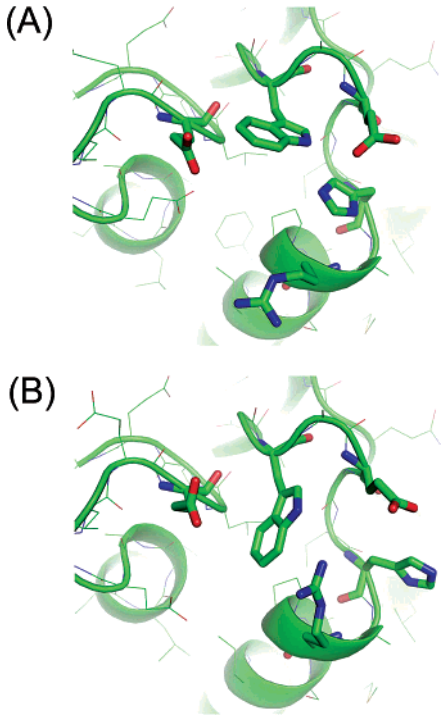

FIGURE 4: Modeled structure of HPr^{sc}. The structure of HPr^{sc} around Trp10. In the first conformation, His15 caps the first α-helix (A), and in the second conformation, His15 points away toward a more solvent-exposed conformation (B).

which are not observed, within the experimental uncertainty in our analysis of $r(t)$ curves. In conclusion, on the basis of the fluorescence results, we cannot rule out the experimental coexistence of two alternative conformations of Trp10, as suggested by the theoretical calculations.

DISCUSSION

HPr^{sc} Forms a Dimeric Species at Low pH. There are several pieces of evidence which suggest that an oligomeric species of HPr^{sc} exists at low pH. First, the high effective power applied during the gradient and the long times used during evolution of the molecule in DOSY experiments (see Materials and Methods), together with the broadening of the signals in the 1D-NMR spectra, suggest an oligomerization event, although not at a large extent to hamper observation of the NMR signals. Second, the presence of a very long correlation time in fluorescence measurements (φ_3 in Table 3). Third, the FTIR experiments described (*19*) suggest the presence of aggregated species at acidic pHs. And finally, we have obtained the theoretical R for a dimeric HPr^{sc} random coil, and we have compared it with that obtained experimentally. The radius of gyration, R_g, for a random coil conformation is $6R_g^2 = 130n$, where n is the number of

residues (*47*). For a fully random coil polypeptide chain of 113 amino acids, as it is the histidine-tagged HPr^{sc}, R_g = 49 Å, and the hydrodynamic radius is $R = 0.655\langle R_g^2\rangle^{1/2}$ (*48*), which leads in HPr^{sc} to 32.4 Å. A monolayer of hydration is accounted by adding 2.8 Å (*40*), yielding a final calculated hydrodynamic radius for the HPr^{sc} random coil of 35.2 Å. This value is lower than that observed at low pH (Tables 1 and 3), but if we use a polypeptide chain of 226 amino acids (a HPr^{sc} dimer), the theoretical value (48.6 Å) is similar to the experimental one. Nevertheless, such values must be taken with caution, since they are estimations, based on the ideal behavior of a random coil (*40*, *47*, *48*).

If we consider that the low-pH species in HPr^{sc} is a dimeric form, it could be hypothesized that the dimeric form resembled the domain swapped species observed, under native conditions, in some members of the HPr family (*49*). We have also modeled the domain-swapped species of the HPr^{sc}, resulting in a species with a main axis of 64 Å (data not shown), larger than that determined experimentally (Table 1). However, the structure modeled had a well-defined structure, and the species at low pH has not tertiary structure and it has lost most of its tertiary structure (*19*); then, although we cannot rule out the presence of a residual population of domain-swapped species in solution at low pH, those putative domain-swapped forms should be highly disordered.

Finally, it is important to note that there is an apparent discrepancy between the data from the two different techniques used, since at the low pHs (2.5 and 3.2), the DOSY-NMR measurements indicate that the protein species have a large hydrodynamic radius (Table 1). Conversely, the fluorescence lifetime measurements and the anisotropy results indicate that, at pH 3.2, the abrupt change has completely occurred (Tables 2 and 3). To rationalize this apparent discrepancy, it must be taken into account that the DOSY measurements were carried out at a larger concentration than fluorescence measurements (an order of magnitude larger at the most diluted concentration used in DOSY experiment), then, if an aggregated species is formed, as the above-described pieces of evidence suggest, accumulation of this species should be favored at higher concentrations (a consequence of the mass-action law), as those used in NMR measurements.

Motional Dynamics of Trp10 in the Different Conformational States of HPr^{sc}. The most feasible model used to analyze the dynamics of tryptophan considers the fast motions as oscillations (torsional vibrations) of an indole ring within a conformational well (*45*). The slow motions include the rotations of the tryptophan residue together with the entire polypeptide chain, with a backbone segment, and rotation of the indole ring about the $C_\alpha-C_\beta$ and $C_\beta-C_\gamma$ bonds. Thus, as a wide class of movements is possible, anisotropy experiments monitor the average rotational diffusion coefficient.

Three fluorescence lifetimes were observed at any of the explored pHs. The absence of a single lifetime, even when HPr^{sc} is well folded (pH 7), indicates that Trp10 was not locked in a single conformation. In addition, the three rotamers in the native state were also observed when the protein was unfolded at low pH. From the longer correlation time at high pHs (around 7.5 ns), we calculated a hydrodynamic radius of about 19.4 Å, similar, taking into account a hydration layer of 2.8 Å (*40*), to that obtained from the diffusion measurements (Table 1). Then, above pH 3, we conclude that Trp10 is monitoring the overall tumbling of the molecule.

The second correlation time observed at high pHs was around 1.4 ns. This short correlation time must be local in nature and depends on the environment of the tryptophan. Independent motions of tryptophan as those observed for NATA in water or in short unstructured peptides show correlation times in the range of 50−500 ps (*27*). The correlation times of the fastest movements observed in Trp10 are an order of magnitude larger, and thus they must represent segmental motions of the protein region where tryptophan is located. The cone angles for these movements had small values, around 20° (Table 3), reflecting local restrictions.

At pH below 3, the movement of the tryptophan monitored two fast local time scales, whose associated cone angles were around 30°, larger than those observed at higher pHs. These findings suggest that the environment around the tryptophan lacks any long-lived side chain packing interaction that could hamper these two independent segmental movements. On the other hand, the existence of a long correlation time at those pHs further suggests the presence of a nonspecifically dimeric collapsed form at low pH.

The value of around 0.25 for the initial anisotropy, r_0, observed at any pH is lower than the fundamental anisotropy of indole at this excitation wavelength [about 0.28 (*27*)]. An ultrafast energy homotransfer between tryptophan residues of different units of proteins cannot be responsible for this initial depolarization, since the protein is a monomer at high pHs (Tables 1−3). The existence of an additional ultrafast motion on the subpicosecond to picosecond time scale, which cannot be observed with our instrument, is likely to be the source of this depolarization.

Folding of HPr^{sc} Starting from Low pH. The time-resolved fluorescence results described here together with the steady-state fluorescence and CD measurements from our previous work (*19*) define four stages in the HPr^{sc} folding with pH. Below pH 3, the protein is unfolded with a solvent-exposed tryptophan residue, and the two segmental correlation times (0.08 and 0.8 ns at pH 2.48) must reflect fast movements. The presence of a very long correlation time, together with the data from DOSY experiments (Table 1), suggests that species at low pH is a dimer.

In the second stage, in a very narrow pH range, lifetime raises abruptly monitoring a sudden variation in the tryptophan local environment, associated to a protein global shape change. At the end of the step (pH ∼3), the anisotropy goes to zero with two rotational correlation times. The longest one (∼7.5 ns) reflects the global motion of the protein. The short correlation time raises at this step, while the cone angles associated to all of those segmental movements diminish (Table 3). These data reflect the increase in the structural order around the tryptophan.

Between pH 3 and pH 6, the anisotropy of the sole tryptophan did not experience large changes; that is, the global shape of the protein and the segmental motion of Trp10 remained practically unaltered. However, the lifetime dropped in a sigmoidal-like fashion, reflecting local changes in the indole environment. Other parameters that have been shown to change in this pH range are (i) the temperature denaturation profile and (ii) the ANS binding (*19*), which

monitors solvent exposure, reflecting the presence of solvent-exposed hydrophobic regions. The value of this pK_a indicates that a/some highly solvent-exposed glutamate residue(s) could be implicated in the process (*50*). A careful inspection of the modeled structure reveals that Glu12 is close enough to Trp10 as to directly quench it, when it is negatively charged (Figure 4). Similar local rearrangements have been observed in other members of the HPr family upon folding from denaturant (*51*).

The fourth and last stage would be above pH 6. Here, the protein adopts the final native state with a dynamic behavior identical to that of previous stages, but with a local environment slightly different. At this stage, ANS is not bound to the protein (*19*).

Taken together, these results suggest that folding of HPr^{sc} occurs, as monitored by the sole tryptophan of the molecule, via a multiple-state equilibrium, with the first species partially unfolded at low pH, forming dimers, followed by a compact native-like species, where some final rearrangements occur around the indole moiety to acquire the proper fold. Since at pH below 3, there was a dimeric species, with no native tertiary form (ref *19* and the NMR experiments here), but some residual secondary structure (*19*), we could hypothesize that those dimeric species could represent a collapsed productive structure which would yield the native fold after conformational rearrangements (*51*, *52*). Since this dimeric species has been observed in a wide concentration range (from micromolar, in the fluorescence experiments, to millimolar, in the NMR experiments), its dissociation constant must be very low, although the folding process yielding the native well-folded protein is reversible (*19*). Thus, we suggest that the presence of this collapsed form helps the process of folding of HPr^{sc} by promoting the existence of native contacts, which would prevent the formation of unproductive aggregated species.

ACKNOWLEDGMENT

We thank Fritz Titgemeyer for the generous gift of the recombinant plasmid encoding the HPr^{SC}. We thank F. N. Barrera and Dr. C. R. Mateo for critical reading of the manuscript and stimulating ideas. We thank the reviewer and a member of the advisory board for their comments. We gratefully thank María T. Garzón, May García, María C. Fuster, and Javier Casanova for excellent technical assistance.

REFERENCES

1. Jaenicke, R., and Seckler, R. (1997) Protein misassembly *in vitro*, *Adv. Protein Chem. 50*, 1−59.
2. Fink, A. L. (1998) Protein aggregation: folding aggregates, inclusion bodies and amyloid, *Folding Des. 3*, 9−23.
3. Wetzel, R. (1996) For protein misassembly, it's the "I" decade, *Cell 86*, 699−702.
4. Silow, M., and Oliveberg, M. (1997) Transient aggregates in protein folding are easily mistaken for folding intermediates, *Proc. Natl. Acad. Sci. U.S.A. 94*, 6084−6086.
5. Pecorari, F., Minard, P., Desmadril, M., and Yon, J. M. (1996) Occurrence of transient multimeric species during the refolding of a monomeric protein, *J. Biol. Chem. 271*, 5720−5726.
6. Fink, A. L. (1995) Compact intermediate states in protein folding, *Annu. Rev. Biophys. Biomol. Struct. 24*, 495−522.
7. Booth, D. R., Sunde, M., Bellotti, V., Robinson, C. V., Hutchisnson, W. L., Fraser, P. E., Hawkins, P. N., Dobson, C. M., Radford, S. E., Blake, C. C. F., and Pepys, M. B. (1997) Instability, unfolding and aggregation of human lysozyme variants underlying amyloid fibrillogenesis, *Nature 385*, 787−793.
8. Lai, Z., Colon, W., and Kelly, J. W. (1996) The acid-mediated denaturation pathway of transthyretin yields a conformational intermediate that can self-assemble into amyloid, *Biochemistry 35*, 6470−6482.
9. Postma, P. W., Lengeler, J. W., and Jacobson, G. R. (1993) Phosphoeneolpyruvate carbohydrate phosphotransferase system of bacteria, *Microbiol. Rev. 57*, 543−594.
10. Meadow, N. D., Fox, D. K., and Roseman, S. (1990) The bacterial phosphoenolpyruvate:glycose phosphotransferase system, *Annu. Rev. Biochem. 59*, 497−542.
11. Titgemeyer, F., Walkenhorst, J., Cui, X., Reizer, J., and Saier, M. H., Jr. (1994) Proteins of the phosphoenolpyruvate:sugar phosphotransferase system in *Streptomyces*: possible involvement in the regulation of antibiotic production, *Res. Microbiol. 145*, 89−92.
12. Titgemeyer, F., Walkenhorst, J., Reizer, J., Stuiver, M. H., Cui, X., and Saier, M. H., Jr. (1995) Identification and characterization of phosphoenolpyruvate:fructose phosphotransferase systems in three *Streptomyces* species, *Microbiology 141*, 51−58.
13. Parche, S., Schmid, R., and Titgemeyer, F. (1999) The PTS system of *Streptomyces coelicolor*: identification and biochemical analysis of a histidine phosphocarrier protein HPr encoded by the gene ptsH, *Eur. J. Biochem. 265*, 308−317.
14. Wittekind, M., Rajagopal, P., Baranchini, B. R., Reizer, J., Saier, M. H., Jr., and Klevitt, R. E. (1992) Solution structure of the phosphocarrier protein HPr from *Bacillus subtilis* by two-dimensional NMR spectroscopy, *Protein Sci. 1*, 1363−1376.
15. Van Nuland, N. A. J., Hangyi, I. W., Van Schaik, R. C., Berendsen, H. J. C., Van Gusteren, W. F., Scheek, R. M., and Robillard, G. T. (1994) The high-resolution structure of the histidine-containing phosphocarrier protein HPr from *Escherichia coli* determined by restrained molecular dynamics from nuclear magnetic resonance nuclear Overhauser effect data, *J. Mol. Biol. 237*, 544−559.
16. Maurer, T., Doker, R., Gorler, A., Hengstenberg, W., and Kalbitzer, H. R. (2001) Three-dimensional structure of the histidine-containing phosphocarrier protein (HPr) from *Enterococcus faecalis* in solution, *Eur. J. Biochem. 268*, 635−644.
17. Herzberg, O., Reddy, P., Sutrin, S., Saier, M. H., Jr., Reizer, J., and Kapafia, G. (1992) Structure of the histidine-containing phosphocarrier protein HPr from *Bacillus subtilis* at 2.0-Å resolution, *Proc. Natl. Acad. Sci. U.S.A. 89*, 2499−2503.
18. Jia, Z., Quail, J. W., Waygood, E. B., and Delbaere, L. T. J. (1993) The 2.0-Å resolution structure of *Escherichia coli* histidine-containing phosphocarrier protein HPr: a redetermination, *J. Biol. Chem. 268*, 22490−22501.
19. Fernández-Ballester, G., Maya, J., Martín, A., Parche, S., Gómez, J., Titgemeyer, F., and Neira, J. L. (2003) The histidine-phosphocarrier protein of *Streptomyces coelicolor* folds by a partially folded species at low pH, *Eur. J. Biochem. 270*, 2254−2267.
20. Pace, C. N., and Scholtz, J. M. (1997) Measuring the conformational stability of a protein, in *Protein Structure* (Creighton, T. E., Ed.) 2nd ed., pp 253−259, Oxford University Press, Oxford.
21. Price, W. S. (1997) Pulse-field gradient nuclear magnetic resonance as a tool for studying translational diffusion: Part I. Basic theory, *Concepts Magn. Reson. 9*, 299−336.
22. Price, W. S. (1998) Pulse-field gradient nuclear magnetic resonance as a tool for studying translational diffusion: Part II. Experimental aspects, *Concepts Magn. Reson. 10*, 197−237.
23. Lapham, J., Rife, J. P., Moore, P. B., and Crothers, D. M. (1997) Measurement of diffusion constants for nucleic acids by NMR, *J. Biomol. NMR 10*, 255−262.
24. James, D. R., and Siemiarczuk, A. (1992) Stroboscopic optical boxcar technique for the determination of fluorescence lifetimes, *Rev. Sci. Instrum. 63*, 1710−1716.
25. Liu, R., Siemiarczuk, A., and Sharom, F. J. (2000) Intrinsic fluorescence of the P-glycoprotein multidrug transporter: sensitivity of tryptophan residues to binding of drugs and nucleotides, *Biochemistry 39*, 14927−14938.
26. Poveda, J. A., Prieto, M., Encinar, J. A., Gonzalez-Ros, J. M., and Mateo, C. R. (2003) Intrinsic tyrosine fluorescence as a tool to study the interaction of the shaker B "ball" peptide with anionic membranes, *Biochemistry 42*, 7124−7132.
27. Lakowicz, J. R. (1999) *Principles of Fluorescence Spectroscopy*, 2nd ed., Kluwer Academic/Plenum Press, New York.
28. Dale, R. E., Chen, L. A., and Brand, L. (1977) Rotational relaxation of the "microviscosity" probe diphenylhexatriene in paraffin oil and egg lecithin vesicles, *J. Biol. Chem. 252*, 2163−2169.

29. Heyn, M. P. (1989) Order and viscosity of membranes: analysis by time-resolved fluorescence depolarization, *Methods Enzymol. 172*, 462−471.
30. Lipari, G., and Szabo, A. (1980) Effect of librational motion on fluorescence depolarization and nuclear magnetic resonance relaxation in macromolecules and membranes, *Biophys. J. 30*, 489−506.
31. Kinoshita, K., Jr., Kawato, S., and Ikegami, A. (1977) A theory of fluorescence polarization decay in membranes, *Biophys. J. 20*, 289−305.
32. Schwede, T., Kopp, J., Guex, N., and Peitsch, M. C. (2003) SWISS-MODEL: an automated protein homology-modeling server, *Nucleic Acids Res. 31*, 3381−3385.
33. Pieper, U., Kapadia, G., Zhu, P. P., Peterkofsky, A., and Herzberg, O. (1995) Structural evidence for the evolutionary divergence of *Mycoplasma* from gram-positive bacteria: the histidine-containing phosphocarrier protein, *Structure 3*, 781−790.
34. Guex, N., and Peitsch, M. C. (1997) SWISS-MODEL and the Swiss-Pdb viewer: an environment for comparative protein modeling, *Electrophoresis 18*, 2714−2723.
35. Guerois, R., Nielsen, J. E., and Serrano, L. (2002) Predicting changes in the stability of proteins and protein complexes: a study of more than 1000 mutations, *J. Mol. Biol. 320*, 369−387.
36. Schymkowitz, J., Borg, J., Stricher, F., Nys, R., Rousseau, F., and Serrano, L. (2005). The FoldX web server: an online force field, *Nucleic Acids Res. 33* (Web Server issue), W382−W388.
37. Laskowski, R. A., Rullmann, J. A. C., MacArthur, M. W., Kaptein, R., and Thronton, J. M. (1996) AQUA and PROCHECK-NMR: programs for checking the quality of proteins structures solved by NMR, *J. Biomol. NMR 8*, 477−486.
38. Cantor, C. R., and Schimmel, P. R. (1980) *Biophysical Chemistry*, W. H. Freeman, New York.
39. Creighton, T. E. (1993) *Proteins. Structures and macromolecular properties*, 2nd ed., W. H. Freeman, New York.
40. Pan, H., Barany, G., and Woodward, C. (1997) Reduced BPTI is collapsed. A pulse field gradient NMR study of unfolded and partially folded bovine pancreatic trypsin inhibitor, *Protein Sci. 6*, 1985−1992.
41. Ross, J. B., Wyssbrod, H. R., Porter, A. R., Schwartz, G. P., Michaels, C. A., and Laws, W. R. (1992) Correlation of tryptophan fluorescence intensity decay parameters with ^{1}H NMR-determined rotamer conformations: [tryptophan2]oxytocin, *Biochemistry 31*, 1585−1594.
42. Gauduchon, P., and Wahl, P. (1978) Pulse fluorimetry of tyrosyl peptides, *Biophys. Chem. 8*, 87−104.
43. Laws, W. R., Ross, J. B., Wyssbrod, H. R., Beechem, J. M., Brand, L., and Sutherland, J. C. (1986) Time-resolved fluorescence and ^{1}H NMR studies of tyrosine and tyrosine analogues: correlation of NMR-determined rotamer populations and fluorescence kinetics, *Biochemistry 25*, 599−607.
44. Tcherkasskaya, O., Knutson, J. R., Bowley, S. A., Frank, M. K., and Gronenborg, A. M. (2000) Nanosecond dynamics of the single tryptophan reveals multi-state equilibrium unfolding of protein GB1, *Biochemistry 39*, 11216−11226.
45. Tcherkasskaya, O., Ptitsyn, O. B., and Knutson, J. R. (2000) Nanosecond dynamics of tryptophans in different conformational states of apomyoglobin proteins, *Biochemistry 39*, 1879−1889.
46. Jia, Z., Vandonselaar, M., Quail, J. W., and Delbaere, L. T. (1993) Active-centre torsion-angle strain revealed in 1.6 Å-resolution structure of histidine-containing phosphocarrier protein, *Nature 361*, 94−97.
47. Tanford, C. (1968) Protein denaturation, *Adv. Protein Chem. 23*, 121−282.
48. Bloomfield, V., Crothers, D., and Tinoco, I., Jr. (1974) Transport phenomena, in *Physical chemistry of nucleic acids*, pp 215−254, Harper & Row, New York.
49. Sridharan, S., Razvi, Scholtz, A., J. M., and Sacchettini, J. C. (2005) The HPr proteins from the thermophile *Bacillus stearothermophilus* can form domain-swapped dimmers, *J. Mol. Biol. 346*, 919−931.
50. Thurkill, R. L., Grimsley, G. R., Scholtz, J. M., and Pace, C. N. (2006) pK_a values of the ionizable groups of proteins, *Protein Sci. 15*, 1214−1218.
51. Azuaga, A. I., Canet, D., Smeenk, G., Berends, R., Titgemeyer, F., Duurken, R., Mateo, P. L., Scheek, R. M., Robillard, G. T., Dobson, C. M., and van Nuland, N. A. J. (2003) Characterization of single-tryptophan mutants of histidine-containing phosphocarrier protein: evidence for local rearrangements during folding from high concentrations of denaturant, *Biochemistry 42*, 4883−4895.
52. Azuaga, A. I., Neira, J. L., and van Nuland, N. A. J. (2005) HPr as a model protein in structure, interaction, folding and stability studies, *Protein Pept. Lett. 12*, 123−137.

BI7002923